Monolithic Integration of Membrane-Based Butt-Jointed Built-in DFB Lasers and p-i-n Photodiodes Bonded on Si Substrate

Daisuke Inoue, Takuo Hiratani, *Student Member, IEEE*, Yuki Atsuji, Takahiro Tomiyasu, Tomohiro Amemiya, *Member, IEEE*, Nobuhiko Nishiyama, *Senior Member, IEEE*, and Shigehisa Arai, *Fellow, IEEE*

***Abstract*—We demonstrate a monolithic integration of lateral-current-injection (LCI)-type membrane-based distributed-feedback (DFB) lasers and p-i-n-photodiodes (PDs) using a butt-jointed built-in (BJB) structure bonded on a Si substrate using benzocyclobutene. The BJB structure to be integrated to the membrane optical devices was prepared by organometallic vapor-phase epitaxy. A threshold current of 280 μA was obtained under a room-temperature continuous-wave condition by adopting a strongly index-coupled DFB laser with a surface grating structure and a λ/4-shift region. A low dark current of 0.8 nA was obtained with the p-i-n-PD at a bias voltage of –1 V, and its photocurrent property coincided with the light output property of the membrane DFB laser.**

***Index Terms*—Distributed-feedback laser, lateral-current injection, membrane laser, optical interconnect, semiconductor laser.**

I. Introduction

OPTICAL interconnects have been adopted in large data centers or super computers [1]. Recently, optical communication has exhibited better performance than electrical interconnection in short range and this trend will continue. Furthermore, we expect the introduction of optical interconnection to on-chip interconnection [2]–[4], which is ultimately a short-reach communication. In the on-chip interconnection technology, the current copper interconnects in the global wire layers limit the performance of large-scale integration (LSI) circuits because of its *RC* delay and heat generation [5], [6]. Therefore, introduction of optical communication to on-chip interconnection is one of the solutions of such problems. In contrast to conventional optical devices for long-haul transmissions, which are required to emit output power from a few milliwatts to tens of milliwatts, the required output power for on-chip interconnection is from a few tens of microwatts to hundreds of microwatts when the minimum receivable power of a p-i-n-photodiode (PD) at a signal speed of 10 Gb/s is considered. In particular, the energy cost of the transmitter must be significantly less than 100 fJ/bit [7]. For this purpose, lasers with ultra-low power consumption, such as vertical-cavity surface-emitting lasers (VCSELs) [8]–[10] and photonic-crystal (PhC) lasers [11]–[13], have been extensively investigated. VCSELs with 45° mirrors have been reported for in-plane optical interconnection [14]. A PhC laser with an extremely low energy cost of 4.4 fJ/bit was demonstrated at a signal speed of 10 Gb/s using an extremely small volume of active region and a high-sensitivity avalanche PD (APD) for a received optical power of approximately -30 dBm (1 μW) [15]. However, the applied voltage of a typical APD is only a few tens of volts, which is not suitable for integration with LSI chips. Thus, adoption of a typical p-i-n-PD will be more realistic for on-chip optical interconnects, and the required optical power will be one order of magnitude higher than that using an APD [16].

We propose membrane distributed-feedback (DFB) lasers as light source for on-chip optical interconnection because the membrane structure, which consists of a thin semiconductor core layer sandwiched by dielectric materials, is advantageous in enhancing not only the optical confinement factor of the active region but also the index-coupling coefficient of the grating [17], [18]. Hence, an ultra-low threshold operation can be realized by a membrane DFB structure [17]. In our previous works, room-temperature continuous-wave (RT-CW) operation [19], stable single-mode operation [20], [21], and CW operation up to 85 °C [22] of a membrane DFB laser were demonstrated under optical pumping. For the current injection-type membrane DFB lasers, we introduced a lateral-current-injection (LCI) structure [23] and realized RT-CW operations of the top air-cladding LCI-Fabry–Perot (FP) lasers [24] and DFB lasers [25], [26]. After improving the internal quantum efficiency of an LCI-type laser [27], [28], an RT-CW operation of an LCI-membrane FP laser [29] and a low-threshold-current (390 μA) operation of an LCI-membrane DFB laser bonded on a Si [30] were demonstrated. For integration of the membrane laser to other optical devices such as a GaInAsP wire waveguide [31] and a lateral junction p-i-n-PD [32], we fabricated a butt-jointed built-in (BJB) structure [33] and obtained a smooth structure prepared by organometallic vapor-phase-epitaxy (OMVPE) regrowth

Manuscript received February 13, 2015; revised April 1, 2015 and May 8, 2015; accepted May 18, 2015. Date of publication May 21, 2015; date of current version July 10, 2015. This work was supported by the JSPS KAKENHI under Grants #24246061, #15H05763, #25709026, and #25420321.

D. Inoue, T. Hiratani, Y. Atsuji, T. Tomiyasu, and N. Nishiyama are with the Department of Electrical and Electronic Engineering, Tokyo Institute of Technology, Tokyo 152-8552, Japan (e-mail: inoue.d.ac@m.titech.ac.jp; hiratani.t.aa@m.titech.ac.jp; atsudi.y.aa@m.titech.ac.jp; tomiyasu.t.aa@m.titech.ac.jp; n-nishi@pe.titech.ac.jp).

T. Amemiya and S. Arai are with the Department of Electrical and Electronic Engineering, Tokyo Institute of Technology, Tokyo 152-8552, Japan and also with the Quantum Nanoelectronics Research Center, Tokyo Institute of Technology, Tokyo 152-8552, Japan (e-mail: amemiya.t.ab@m.titech.ac.jp; arai@pe.titech.ac.jp).

Color versions of one or more of the figures in this paper are available online at http://ieeexplore.ieee.org.

Digital Object Identifier 10.1109/JSTQE.2015.2435898

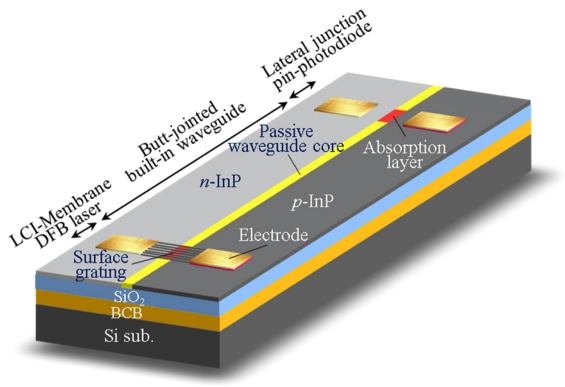

Fig. 1. Schematic diagram of a fabricated device. The λ/4-shifted LCI-membrane DFB laser and lateral junction p-i-n-PD are connected by a BJB waveguide.

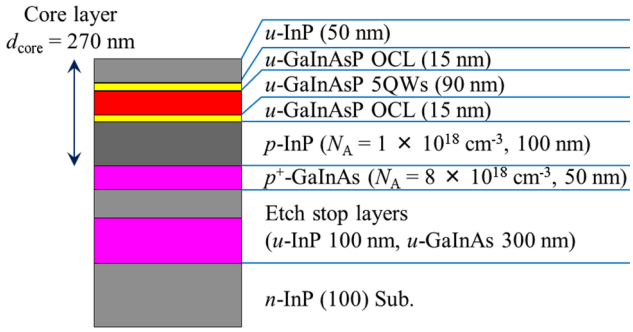

Fig. 2. Schematic diagram of the initial wafer structure.

method [34]. A sub-milliampere threshold current operation of an LCI-membrane DFB laser with a BJB waveguide was realized [35]. However, integration of the LCI-membrane DFB laser and p-i-n-PD has not yet been demonstrated.

In this paper, we present a monolithic integration of an LCI-membrane DFB laser and a lateral junction p-i-n-PD using a BJB structure bonded on a Si substrate, as shown in Fig. 1. Section II describes the fabrication method of the membrane BJB structure for smooth surface with good connection between the active and passive waveguides. Section III discusses the device structure and fabrication process. Section IV presents the experimental results of the fabricated device.

II. Preparation of Membrane BJB Structure

Because the scattering loss of a membrane structure is rather sensitive to flatness owing to its strong optical confinement in the semiconductor core layer, the section interface should be smoothly connected for efficient coupling between sections in a circuit. In this paper, the passive waveguide consists of a u-$Ga_{0.21}In_{0.79}As_{0.49}P_{0.51}$ ($\lambda_g = 1220$ nm) core with InP side cladding layers to form a similar waveguide structure in the active region. Fig. 2 shows the schematic diagram of the initial wafer structure, which consists of etch-stop layers (300-nm-thick u-GaInAs and 100-nm-thick u-InP), a 50-nm-thick p^+-GaInAs contact layer (Be-doped, $N_A = 8 \times 10^{18}\text{cm}^{-3}$), a 100-nm-thick p-InP cap layer (Be-doped, $N_A = 1 \times 10^{18}\text{cm}^{-3}$), 90-nm-thick u-GaInAsP five quantum wells (5QWs) ($\lambda_g = 1520$ nm) sandwiched by 15-nm-thick u-$Ga_{0.21}In_{0.79}As_{0.49}P_{0.51}$ optical confinement layers, and a 50-nm-thick u-InP cap layer. The 5QWs, which consist of five 1% compressively strained 6-nm-thick u-$Ga_{0.22}In_{0.78}As_{0.81}P_{0.19}$, are sandwiched between 0.15% tensile-strained 10-nm-thick u-$Ga_{0.26}In_{0.74}As_{0.49}P_{0.51}$ barrier layers. These epitaxial layers were grown by gas-source molecular beam epitaxy on an n-InP (1 0 0) substrate. The total thickness of the core layer is 270 nm. First, the active regions were covered with a 50-nm-thick SiO_2 mask deposited by plasma-enhanced chemical vapor deposition (PECVD). The mask shape is 10-μm wide and has a 20–300-μm-long square shape defined by photolithography. Then, the u-InP cap layer was etched by CH_4/H_2 reactive ion etching (RIE). The revealed GaInAsP layers were selectively etched by wet chemical using a solution of H_2SO_4:H_2O_2:H_2O = 1:1:40 at 20 °C for 8 min. Then, a passive waveguide layer was selectively regrown by OMVPE under three different growth conditions, as listed in Table I. Fig. 3 shows the scanning electron microscope (SEM) image of the fabricated BJB structure observed from the $[0\ 1\ \bar{1}]$ direction. The GaInAsP core layer in the passive section is directly joined to the 5QWs, whereas the surface of the u-InP layer in the passive section is slightly (~20 nm) higher than that in the active section. The photoluminescence (PL) intensity value of the GaInAsP passive waveguide layer was measured to be the same as that of a passive waveguide layer grown on an n-InP substrate, and the PL peak wavelength was 1.22 μm in both cases [34].

TABLE I
OMVPE Growth Conditions of Waveguide Layer

	Material	Thickness (nm)	Time (min)	Growth Rate (nm/min)	Temperature (°C)
Step 1	u-InP	9	0.5	18	600
Step 2	u-GaInAsP	150	8	22	650
Step 3	u-InP	18	1	18	650

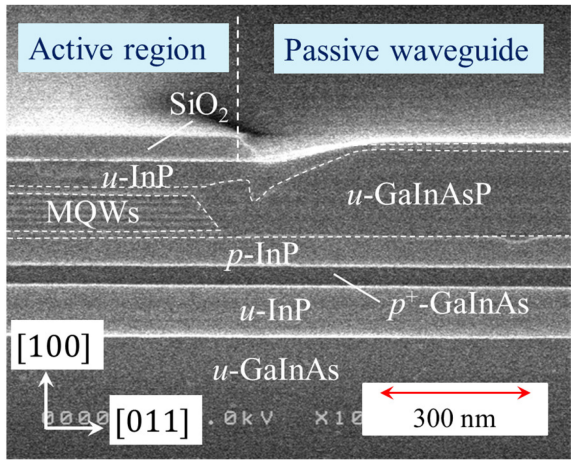

Fig. 3. SEM image of the membrane BJB structure prepared by OMVPE regrowth observed from the $[0\ 1\ \bar{1}]$ direction.

III. Fabrication Process and Device Structure

Fig. 4 shows a schematic diagram of a λ/4-shifted LCI-membrane DFB laser and a lateral junction p-i-n-PD connected

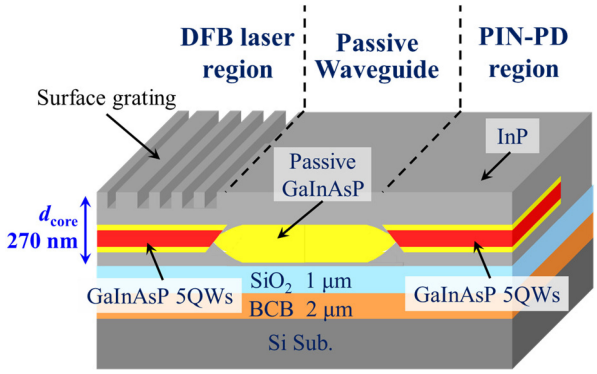

Fig. 4. Schematic diagram of the cross section.

by a BJB waveguide. The p-i-n-PD has a multiple QW (MQW) absorption layer, which is the same as the active layer of the DFB laser section. A λ/4 phase shift in the DFB laser was introduced to achieve a compact cavity length and a stable single-mode operation. The device fabrication was initiated by selective-area regrowth of the waveguide layer by OMVPE, as explained in Section II. Next, a second-step regrowth of *n*-InP ($N_D = 4 \times 10^{18}\mathrm{cm}^{-3}$) and *p*-InP ($N_A = 4 \times 10^{18}\mathrm{cm}^{-3}$) layers was carried out to form a lateral p-i-n junction structure. After the third-step regrowth process, a 1-μm-thick SiO_2 cladding layer was deposited by PECVD, and the wafer was bonded to a Si host substrate using a benzocyclobutene (BCB) adhesive layer. Although there is a report on good bonding using only BCB layer [36], the SiO_2 layer improved the reproducibility of bonding process in our experiments especially for wafer scale bonding without void at the interface. Subsequently, the InP substrate side and etch-stop layers were removed by polishing and selective chemical etching, respectively, to expose the p^+-GaInAs contact layer on the bonded wafer. The *p*-contact layer in the unnecessary region was removed by selective wet chemical etching, and the *p*-InP cap layer in the *n*-side electrode region was etched by CH_4/H_2 RIE. Then, a Ti/Au electrode was deposited by electron-beam evaporation. A grating mask pattern covered with SiO_2 was formed on the laser section using electron-beam (EB) lithography. The exposed grating pattern was 120-nm-wide and 298-nm-grating period. The grating was formed over the active region stripe across 7 μm length. The electron beam dose condition was 180 μC/cm^2. To obtain same pattern width on InP substrate, the exposure pattern width on membrane sample needs approximately 1.25 times wider, because the back scattering on the membrane sample was smaller due to low electron density of cladding layers. The alignment was performed by using Ti/Au cross-mark which was simultaneously deposited with electrodes. Subsequently, the InP cap layer was etched by wet chemical etching. Then, the substrate was cleaved into a bar form at the passive waveguide section. The cleaving was performed by using an automated wafer scriber. We have obtained the cavity length dependence of differential quantum efficiency from the Fabry–Perot lasers fabricated by the same cleaving method reported in the previous work [29]. The cleaved facet had no antireflection coating; hence, the facet reflectivity was calculated to be approximately 20% for this membrane structure.

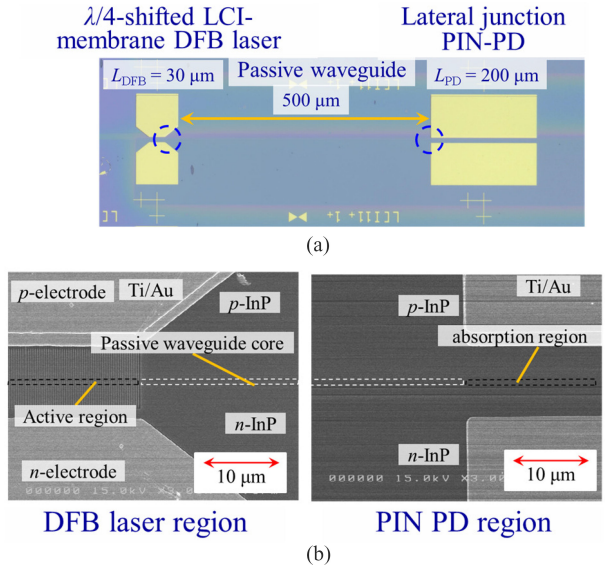

Fig. 5. Structure of the fabricated device. (a) Optical microscope image of the top view. (b) SEM images of the top view. *Left*: DFB laser region. *Right*: p-i-n-PD region.

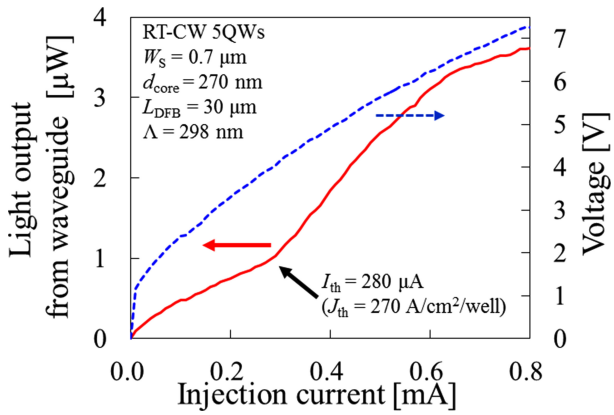

Fig. 6. Light output and voltage-current characteristics of λ/4-shifted LCI-membrane DFB laser.

Fig. 5(a) shows an optical microscope image of the top view of the fabricated device. The stripe width of these devices was 0.7 μm, which satisfies a single-transverse-mode condition. The cavity length of the λ/4-shifted LCI-membrane DFB laser L_{DFB} was 30 μm. The length of the passive waveguide section was 500 μm, and the length of the p-i-n-PD L_{PD} was 200 μm. By considering that the optical confinement factor of the 5 QWs is 13% for a core thickness of 270 nm [18] and the absorption coefficient of the QW is $6000\,\mathrm{cm}^{-1}$, the required length of the p-i-n-PD L_{PD} for 90% absorption of the input power was calculated to be only 30 μm. Fig. 5(b) shows SEM images of the DFB laser and p-i-n-PD regions. We confirmed that surface grating was accurately formed in the laser region.

IV. Measurements Results

The light output of the laser was measured from a facet cleaved at the waveguide section with a length of approximately 500 μm, which is the opposite facet to the p-i-n-PD. Fig. 6 shows the light–current and voltage–current characteristics of

the λ/4-shifted LCI-membrane DFB laser. A threshold current $I_{\rm th}$ of 280 μA and an external differential quantum efficiency η_d of 1% (rear waveguide output) were obtained. The differential resistance at threshold current was 5.4 kΩ for the 30-μm-long device. The distance from the electrodes to the edge of the active region was approximately 3 μm. The reason of high differential resistance was attributed to an unintentional impurity existence of Si and C at the interface between Be-doped InP and regrown Zn-doped InP confirmed by secondary-ion-mass-spectrometry (SIMS). Therefore, by growing the p-InP layer on p^+-GaInAs contact layer to avoid n-type doping of InP, the differential resistance could be reduced to several hundred ohms for the device with the same cavity length. The roll-off in light-output characteristic was considered to be induced by joule heating, because the self-heating has small effects if low-threshold current operation is achieved [37]. The threshold current density $J_{\rm th}$ was 1350 A/cm^2 (270 A/cm^2/well), which was approximately three times higher than that (90 A/cm^2/well) of the longer cavity (100 μm) device fabricated on the same wafer. This poor threshold current as well as the low η_d may be attributed to a leakage current between the DFB laser and the loss of the 500-μm-long passive waveguide section because $\eta_d = 22\%/\text{facet}$ was obtained for the LCI-membrane FP cavity lasers [29]. In order to achieve the target output power for error free operation of p-i-n-PD, introduction of wire waveguide structure for reducing absorption loss [31], distributed-reflector structure for single directional output [38] will offer the significant improvements.

Fig. 7(a) and (b) show the lasing spectrum for the device with cavity length of 30 and 100 μm, respectively. In Fig. 7(a), the lasing wavelength was 1536 nm, and a side-mode (or submode) suppression ratio (SMSR) of 30 dB was obtained at a bias current of 700 μA. The stopband could not be observed from the measurement of 30-μm-long device. From a lasing spectrum of another device with the cavity length of 100 μm as shown in Fig. 7(b), the stopband width was observed to be 35 nm which corresponded to an index-coupling coefficient κ_i of approximately 1600 cm^{-1}. The lasing mode at the center of the stopband (1549 nm) indicates the effect of the λ/4-shifted DFB cavity. Several lasing modes observed in the shorter wavelength side of the stopband also corresponds to the resonant (and lasing) modes defined by the DFB grating. The stronger mode than the mode at the center of the stopband was due to mismatching of the gain peak wavelength. By adopting this κ value, the grating coupling strength $\kappa L_{\rm DFB}$ of the 30-μm-long DFB region was 4.8, which was sufficiently high to suppress the threshold current density similar to that of the long cavity device. Therefore, we believe that the increased threshold current density can be attributed to the leakage current or poor grating coupling strength $\kappa L_{\rm DFB}$ due to non-uniformity.

Fig. 8 shows the cavity length dependence of obtained threshold currents for LCI-membrane DFB lasers with and without λ/4-shift fabricated on same wafer, where the solid and dashed lines show theoretical curves for them by assuming an internal quantum efficiency (η_i) of 75% which was obtained from the cavity length dependence of an external differential quantum efficiency of membrane Fabry–Perot cavity lasers [29]. The reduction of threshold current by shortening the cavity length was

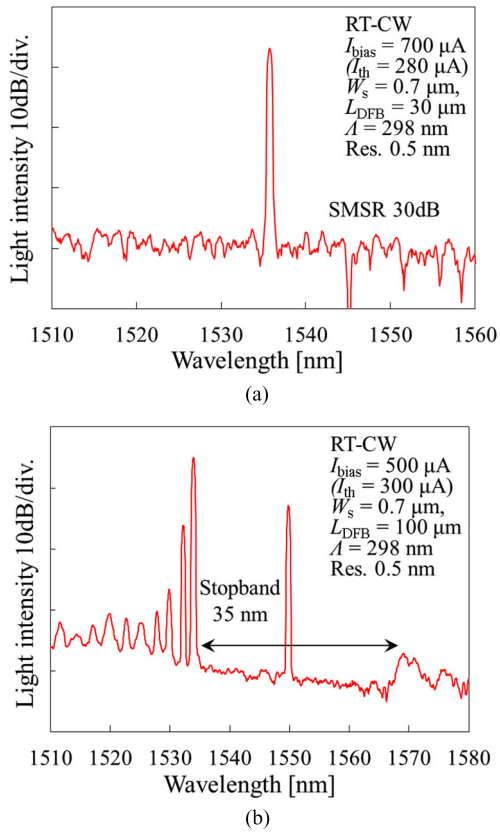

Fig. 7. Lasing spectrum of λ/4-shifted LCI-membrane DFB laser for the (a) $L_{\rm DFB} = 30$ μm and (b) $L_{\rm DFB} = 100$ μm.

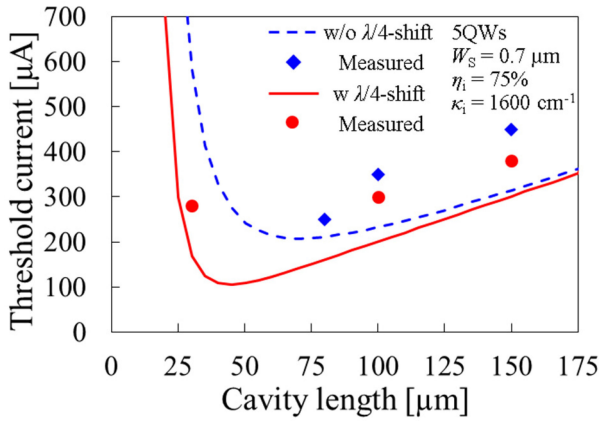

Fig. 8. Cavity length dependence of threshold current of LCI-membrane DFB laser with and without λ/4 phase shift. The solid and dashed lines show theoretical curves. Plots show obtained values from the measurement results.

confirmed. As for the lasers without λ/4-shift, the lasing operation was not obtained for cavity length of shorter than 80 μm. By contrast, the λ/4-shifted lasers operated with 30-μm-long cavity which was one-fifth of length of previous work. We can expect the minimum threshold current of 100 μA by suppressing the leakage current.

Next, we measured the optical transmission characteristics of the fabricated optical link. The photocurrent of the p-i-n-PD integrated with the λ/4-shifted DFB laser through a 500-μm-long BJB passive waveguide was measured. The responsivity of the

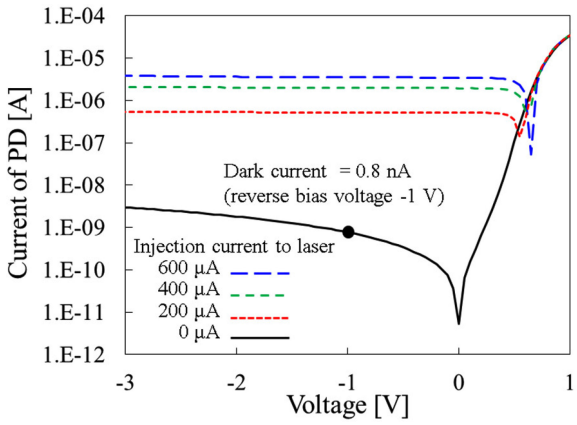

Fig. 9. Photocurrent as a function of bias voltage of the PD for various injection currents to the membrane DFB laser.

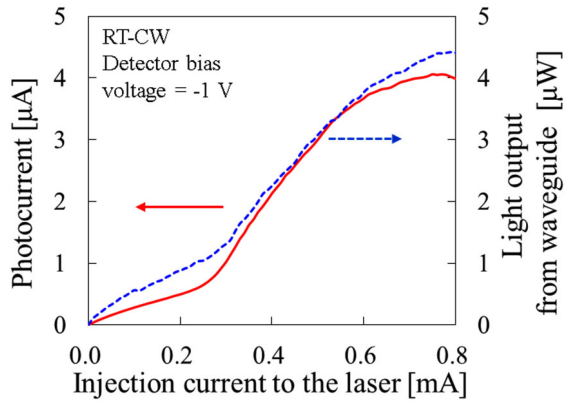

Fig. 10. Photocurrent-injection current to the laser characteristics.

p-i-n-PD was separately measured for another device with the same device length and stripe width. The measurement was carried out by coupling an external wavelength-tunable laser source to the BJB passive waveguide of PD by using a spherical-lensed single-mode polarization-maintaining fiber. The polarization of output from fiber was controlled to be TE-mode. The coupling efficiency between passive waveguide and lensed fiber was estimated to be 2.3% by comparing the light output power of integrated DFB laser from a passive waveguide detected by commercial vertically illuminated p-i-n-PD with the its power collected by the lensed fiber. As a result, the responsivity of 0.8 W/A was estimated at a wavelength of 1550 nm. Fig. 9 shows the photocurrent versus voltage characteristics of the p-i-n-PD for various injection currents to the λ/4-shifted DFB laser. The dark current of the PD was 0.8 nA at a bias voltage of −1 V. The photocurrent was almost independent of the reverse bias voltage up to an injection current of 600 μA.

Fig. 10 shows the photocurrent of the p-i-n-PD versus injection current to the DFB laser characteristics with a p-i-n-PD bias voltage of −1 V, where the blue and red lines indicate the light output characteristic of the DFB laser and the photocurrent, respectively. In this measurement, both *n*-side electrodes were set as a common ground, and the isolation resistance between the *p*-side electrodes of the laser and the PD was approximately 80 MΩ. Therefore, the leakage current between the laser and the PD had little effect on the measured results. At a laser threshold current of 280 μA, a kink in the photocurrent was observed, and a photocurrent of approximately 3 μA was obtained for approximately 3 μW light output of the DFB laser. When we assumed that the BJB passive waveguide (500-μm long) loss at the laser output side was the same as that between the DFB laser and the p-i-n-PD (500-μm long), the input light power to the p-i-n-PD was approximately 1.25 times higher than the light output of the DFB laser because the residual reflectivity of the cleaved facet was approximately 20%. Hence, the effective input power to the p-i-n-PD was calculated to be 3.75 μW, and the quantum efficiency of the p-i-n-PD was calculated to be 64%. In the future, the optical loss of a BJB passive waveguide should be measured to clarify the quantum efficiency of the p-i-n-PD. In addition, the high-speed modulation characteristics of the membrane DFB laser as well as the high-speed performance of this optical link should be investigated.

V. Conclusion

In this paper, we demonstrated a monolithic integration of a λ/4-shifted LCI-membrane DFB laser, a passive waveguide, and a p-i-n-PD using a BJB structure on a Si substrate toward on-chip optical interconnection. The fabrication of the BJB structure was investigated for integration of membrane-based optical devices. A flat and smooth BJB regrown structure was obtained by controlling the OMVPE regrowth conditions and the mesa shape of the active region. Integration of a λ/4-shifted LCI-membrane DFB laser and a p-i-n-PD was performed. With regard to the λ/4-shifted LCI-membrane DFB laser, a threshold current $I_{\rm th}$ of 280 μA and a single-mode operation with a SMSR of 30 dB were realized for the cavity length of 30 μm and stripe width of 0.7 μm. Optical transmission between the laser and PD was confirmed. The light output of the λ/4-shifted DFB laser was successfully detected by the integrated p-i-n-PD. These results show that a membrane-based optical interconnection using DFB laser and p-i-n-PD is promising for on-chip optical interconnections.

References

[1] A. Benner, "Optical interconnect opportunities in supercomputers and high end computing," presented at the Opt. Fiber Commun./Nat. Fiber Opt. Electron. Commun. Conf., Los Angeles, CA, USA, Mar. 2012, Paper OTu2B4.

[2] D. A. B. Miller, "Rationale and challenges for optical interconnects to electronic chips," *Proc. IEEE*, vol. 88, no. 6, pp. 728–749, Jun. 2000.

[3] G. Chen *et al.*, "Prediction of CMOS compatible on-chip optical interconnect," *Integr. VLSI J.*, vol. 40, no. 4, pp. 434–446, Jul. 2007.

[4] K. Ohashi *et al.*, "On-chip optical interconnect," *Proc. IEEE*, vol. 97, no. 7, pp. 1186–1198, Jul. 2009.

[5] P. Kapur, J. P. McVittie, and K. C. Saraswat, "Technology and reliability constrained future copper interconnects—Part I: Resistance modeling," *Trans. Electron Devices*, vol. 49, no. 4, pp. 590–597, Apr. 2002.

[6] P. Kapur, G. Chandra, J. P. McVittie, and K. C. Saraswat, "Technology and reliability constrained future copper interconnects—Part II: Performance implications," *Trans. Electron. Devices*, vol. 49, no. 4, pp. 598–604, Apr. 2002.

[7] D. A. B. Miller, "Device requirements of optical interconnects to silicon chips," *Proc IEEE*, vol. 97, no. 7, pp. 1166–1185, Jul. 2009.

[8] P. Moser *et al.*, "81 fJ/bit energy-to-data ratio of 850 nm vertical-cavity surface emitting lasers for optical interconnects," *Appl. Phys. Lett.*, vol. 98, no. 23, pp. 231106–1–231106-3, Jun. 2011.

[9] S. Imai *et al.*, "Recorded low power dissipation in highly reliable 1060-nm VCSELs for 'Green' optical interconnection," *IEEE J. Sel. Topics Quantum Electron.*, vol. 17, no. 6, pp. 1614–1620, Nov./Dec. 2011.
[10] A. Kasukawa, "VCSEL technology for green optical interconnects," *IEEE Photon. J.*, vol. 4, no. 2, pp. 642–646, Apr. 2012.
[11] B. Ellis *et al.*, "Ultralow-threshold electrically pumped quantum-dot photonic-crystal nanocavity laser," *Nature Photon.*, vol. 5, no. 5, pp. 297–300, May 2011.
[12] S. Matsuo *et al.*, "Ultralow operating energy electrically driven photonic crystal lasers," *IEEE J. Sel. Topics Quantum Electron.*, vol. 19, no. 4, p. 4900311, Jul./Aug. 2013.
[13] K. Takeda *et al.*, "Heterogeneously integrated photonic-crystal lasers on silicon for on/off chip optical interconnects," *Opt. Exp.*, vol. 23, no. 2, pp. 702–708, Jan. 2015.
[14] C.-T. Chen *et al.*, "Chip-level 1 × 2 optical interconnects using polymer vertical splitter on silicon substrate," *IEEE Photon. J.*, vol. 6, no. 2, p. 7900410, Apr. 2014.
[15] K. Takeda *et al.*, "Few-fJ/bit data transmissions using directly modulated lambda-scale embedded active region photonic-crystal lasers," *Nature Photon.*, vol. 7, no. 7, pp. 569–575, Jul. 2013.
[16] S. Arai, N. Nishiyama, T. Maruyama, and T. Okumura, "GaInAsP/InP membrane lasers for optical interconnects," *IEEE J. Sel. Topics Quantum Electron.*, vol. 17, no. 5, pp. 1381–1389, Sep./Oct. 2011.
[17] S. Sakamoto *et al.*, "Strongly index-coupled membrane BH-DFB lasers with surface corrugation grating," *IEEE J. Sel. Topics Quantum Electron.*, vol. 13, no. 5, pp. 1135–1141, Sep. 2007.
[18] T. Okumura, T. Koguchi, H. Ito, N. Nishiyama, and S. Arai, "Injection-type GaInAsP/InP membrane buried heterostructure distributed feedback laser with wirelike active regions," *Appl. Phys. Exp.*, vol. 4, no. 4, pp. 042101–1–042101-3, Apr. 2011.
[19] T. Okamoto, N. Nunoya, Y. Onodera, S. Tamura, and S. Arai, "Continuous wave operation of optically pumped membrane DFB laser," *Electron. Lett.*, vol. 37, no. 24, pp. 1455–1457, Nov. 2001.
[20] T. Okamoto, N. Nunoya, Y. Onodera, S. Tamura, and S. Arai, "Low-threshold single-mode operation of membrane BH-DFB lasers," *Electron. Lett.*, vol. 38, no. 23, pp. 1444–1446, Nov. 2002.
[21] T. Okamoto *et al.*, "Optically pumped membrane BH-DFB lasers for low-threshold and single-mode operation," *IEEE J. Sel. Topics Quantum Electron.*, vol. 9, no. 5, pp. 1361–1366, Sep./Oct. 2003.
[22] S. Sakamoto *et al.*, "85 °C continuous-wave operation of GaInAsP/InP-membrane buried heterostructure distributed feedback lasers with polymer cladding layer," *Jpn. J. Appl. Phys.*, vol. 46, no. 47, pp. L1155–L1157, Nov. 2007.
[23] K. Oe, Y. Noguchi, and C. Caneau, "GaInAsP lateral current injection lasers on semi-insulating substrates," *IEEE Photon. Technol. Lett.*, vol. 6, no. 4, pp. 479–481, Apr. 1994.
[24] T. Okumura, H. Ito, D. Kondo, N. Nishiyama, and S. Arai, "Continuous wave operation of thin film lateral current injection lasers grown on semi-insulating InP substrate," *Jpn. J. Appl. Phys.*, vol. 49, no. 4, pp. 040205–1–040205-3, Apr. 2010.
[25] T. Shindo *et al.*, "GaInAsP/InP lateral-current-injection distributed feedback laser with a- Si surface grating," *Opt. Exp.*, vol. 19, no. 3, pp. 1884–1891, Jan. 2011.
[26] T. Shindo *et al.*, "Lateral-current-injection distributed feedback laser with surface grating structure," *IEEE J. Sel. Topics Quantum Electron.*, vol. 17, no. 5, pp. 1175–1182, Sep./Oct. 2011.
[27] M. Futami *et al.*, "GaInAsP/InP lateral current injection laser with uniformly distributed quantum wells structure," *IEEE Photon. Technol. Lett.*, vol. 24, no. 11, pp. 888–890, Jun. 2012.
[28] M. Futami *et al.*, "Improved quantum efficiency of GaInAsP/InP top air-clad lateral current injection lasers," in *Proc. IEEE Opt. Interconnects Conf.*, May 2012, pp. 34–35.
[29] D. Inoue *et al.*, "Room-temperature continuous-wave operation of GaInAsP/InP lateral-current-injection membrane laser bonded on Si substrate," *Appl. Phys. Exp.*, vol. 7, no. 7, pp. 072701–1–072701-4, Jul. 2014.
[30] Y. Atsuji *et al.*, "Low-threshold-current operation of lateral current injection membrane distributed-feedback laser bonded on Si," presented at the 26th Int. Conf. Indium Phosphide Related Mater., Montpellier, France, May 2014, Paper WeD2-2.
[31] J. Lee *et al.*, "Low loss GaInAsP wire waveguide on Si substrate with benzocyclobutene adhesive wafer bonding for membrane photonic circuits," *Jpn. J. Appl. Phys.*, vol. 51, no. 4, pp. 042201–1–042201-5, Apr. 2012.
[32] T. Shindo *et al.*, "10 Gbps operation of top air-clad lateral junction waveguide-type photodiodes," *Jpn. J. Appl. Phys.*, vol. 52, no. 11, pp. 118002–118002–1-3, Nov. 2013.
[33] Y. Abe, K. Kishino, Y. Suematsu, and S. Arai, "GaInAsP/InP integrated laser with butt-jointed built-in distributed-Bragg-reflection waveguide," *Electron. Lett.*, vol. 17, no. 25, pp. 945–947, Dec. 1981.
[34] D. Inoue *et al.*, "Butt-joint built-in (BJB) structure for membrane photonic integration," presented at the 25th Int. Conf. Indium Phosphide Related Mater., Kobe, Japan, May 2013, Paper TuD3-6.
[35] D. Inoue *et al.*, "GaInAsP/InP lateral-current-injection membrane DFB laser integrated with GaInAsP waveguides on Si substrate," presented at the 24th IEEE Int. Semiconductor Laser Conf., Mallorca, Spain, Sep. 2014, Paper MB-2.
[36] S. Stankovic *et al.*, "Hybrid III–V/Si distributed-feedback laser based on adhesive bonding," *IEEE Photon. Technol. Lett.*, vol. 24, no. 23, pp. 2155–2158, Dec. 2012.
[37] K. Doi *et al.*, "Thermal analysis of lateral-current-injection membrane distributed feedback laser," *IEEE J. Quantum Electron.*, vol. 50, no. 5, pp. 321–326, May 2014.
[38] K. Ohira, T. Murayama, S. Tamura, and S. Arai, "Low-threshold and high-efficiency operation of distributed reflector lasers with width-modulated wirelike active regions," *IEEE J. Sel. Topics Quantum Electron.*, vol. 11, no. 5, pp. 1162–1168, Sep./Oct. 2005.

Daisuke Inoue was born in Okayama, Japan, in 1990. He received the B.E. degree in electrical and electronic engineering from the Tokyo Institute of Technology, Tokyo, Japan, in 2013, where he is currently working toward the M.E. degree in electrical and electronic engineering.

His current research interests include membrane-based photonic devices for optical interconnection.

Mr. Inoue is a Student Member of the Institute of Electronics, Information and Communication Engineers, and the Japan Society of Applied Physics.

Takuo Hiratani (S'13) was born in Ishikawa, Japan, in 1990. He received the B.E. degree in electrical and electronic engineering from Kanazawa University, Ishikawa, Japan, in 2012 and the M.E. degree in electrical and electronic engineering from the Tokyo Institute of Technology, Tokyo, Japan, in 2014, where he is currently working toward the Ph.D. degree in electrical and electronic engineering.

His current research interests include membrane-based photonic devices for optical interconnection.

Mr. Hiratani is a Student Member of the Institute of Electronics, Information and Communication Engineers and the Japan Society of Applied Physics.

Yuki Atsuji was born in Tokyo, Japan, in 1991. He received the B.E. degree from the University of Electro-Communications, Tokyo, Japan, in 2013. He is currently working toward the M.E. degree in the Department of Electrical and Electronic Engineering, Tokyo Institute of Technology, Tokyo, Japan.

His current research interests include membrane-based photonic devices for optical interconnection.

Mr. Atsuji is a Student Member of the Japan Society of Applied Physics.

Takahiro Tomiyasu was born in Fukuoka, Japan, in 1992. He is currently working toward the B.E. degree in the Department of Electrical and Electronic Engineering, Tokyo Institute of Technology, Tokyo, Japan.

His current research interests include membrane-based DFB lasers for optical interconnection

Mr. Tomiyasu is a Student Member of the Institute of Electronics, Information, and Communication Engineers.

Tomohiro Amemiya (S'06–M'09) received the B.S. and Ph.D. degrees in electronic engineering from the University of Tokyo, Tokyo, Japan, in 2004 and 2009, respectively.

In 2009, he moved to the Quantum Electronics Research Center, Tokyo Institute of Technology, where he is currently an Assistant Professor. His research interests include physics of semiconductor light-controlling devices, metamaterials for optical frequencies, magneto-optical devices, and the technologies for fabricating these devices.

Dr. Amemiya is a Member of the Optical Society of America, the American Physical Society, and the Japan Society of Applied Physics. He received the 2007 IEEE Photonics Society Annual Student Paper Award, the 2008 IEEE Photonics Society Graduate Student Fellowship, and the 2012 Konica Minolta Imaging Award.

Nobuhiko Nishiyama (M'01–SM'07) was born in Yamaguchi, Japan, in 1974. He received the B.E., M.E., and Ph.D. degrees from the Tokyo Institute of Technology, Tokyo, Japan, in 1997, 1999, and 2001, respectively.

During his Ph.D. work, he demonstrated single-mode 0.98- and 1.1-μm VCSEL arrays with stable polarization using misoriented substrates for high-speed optical networks as well as MOCVD-grown GaInNAs VCSELs. He joined Corning, Inc., New York, NY, USA, in 2001 and worked with the Semiconductor Technology Research Group. At Corning, he worked on several subjects, including short-wavelength lasers, 1060-nm DFB/DBR lasers, and long-wavelength InP-based VCSELs. Since 2006, he has been an Associate Professor with the Tokyo Institute of Technology. His current main interests include transistor lasers, silicon photonics, III–V silicon hybrid optical devices, and terahertz–optical signal conversions involving optics–electronics–radio integration circuits.

Dr. Nishiyama is a Member of the Japan Society of Applied Physics, IEICE, and IEEE Photonics Society. He received the Excellent Paper Award from the Institute of Electronics, Information and Communication Engineers of Japan in 2001 and the Young Scientists Prize in the Commendation for Science and Technology from the Minister of Education, Culture, Sports, Science and Technology in 2009.

Shigehisa Arai (M'83–SM'06–F'10) was born in Kanagawa, Japan, in 1953. He received the B.E., M.E., and D.E. degrees in electronics from the Tokyo Institute of Technology, Tokyo, Japan, in 1977, 1979, and 1982, respectively.

During his Ph.D. work, he demonstrated room-temperature continuous-wave operations of 1.11–1.67-μm-long wavelength lasers fabricated by liquid-phase epitaxy as well as their single-mode operations under rapid direct modulation. He joined the Department of Physical Electronics, Tokyo Institute of Technology, as a Research Associate in 1982, and was with AT&T Bell Laboratories, Holmdel, NJ, USA, as a Visiting Researcher from 1983 to 1984, on leave from the Tokyo Institute of Technology. He became a Lecturer in 1984, an Associate Professor in 1987, and a Professor in 1994 with the Research Center for Quantum Effect Electronics and the Department of Electrical and Electronic Engineering, Tokyo Institute of Technology. Since 2004, he has been a Professor with the Quantum Nanoelectronics Research Center, Tokyo Institute of Technology. His research interests include photonic integrated devices such as dynamic-single-mode and wavelength-tunable semiconductor lasers, semiconductor optical amplifiers, and optical switches/modulators. His current research interests also include studies of low-damage and cost-effective processing technologies of ultrafine structures for high-performance lasers and photonic integrated circuits on silicon platforms.

Dr. Arai is a Member of the Optical Society of America, the Institute of Electronics, Information and Communication Engineers, and the Japan Society of Applied Physics. He received the Excellent Paper Award from the IEICE of Japan in 1988, the Michael Lunn Memorial Award from the Indium Phosphide and Related Materials Conference in 2000, prizes for science and technology including a Commendation for Science and Technology from the Minister of Education, Culture, Sports, Science and Technology in 2008, an Electronics Society Award and an Achievement Award from IEICE in 2008 and 2011, respectively, and a JSAP Fellowship in 2008.